

# Ocular Pharmacokinetics of Therapeutic Antibodies Given by Intravitreal Injection: Estimation of Retinal Permeabilities Using a 3-Compartment Semi-Mechanistic Model

Laurence A. Hutton-Smith,<sup>\*,†</sup> Eamonn A. Gaffney,<sup>†</sup> Helen M. Byrne,<sup>†</sup> Philip K. Maini,<sup>†</sup> Kapil Gadkar,<sup>‡</sup> and Norman A. Mazer<sup>\*,¶</sup>

<sup>†</sup>*Wolfson Centre For Mathematical Biology, Mathematical Institute, Andrew Wiles Building, University of Oxford, Radcliffe Observatory Quarter, Woodstock Road, Oxford, OX2 6GG, UK*

<sup>‡</sup>*Department of Preclinical and Translational Pharmacokinetics, Genentech, Inc., South San Francisco, California, United States*

<sup>¶</sup>*Clinical Pharmacology, Roche Pharma Research Early Development, Roche Innovation Center Basel, Bldg. 663/ 2130.12, Hochstrasse 16, 4070, Basel, Switzerland*

E-mail: laurence.hutton-smith@pmb.ox.ac.uk; norman.mazer@roche.com

## Abstract

Intravitreally (IVT) injected macromolecules for the treatment of age-related macular degeneration must permeate through the inner limiting membrane (ILM) into the retina and through the retinal pigment epithelium (RPE) to enter the choroid. A quantitative understanding of intra-ocular transport mechanisms, elimination pathways and the effect of molecular size, is currently incomplete. We present a semi-mechanistic, 3-compartment (retina, vitreous and aqueous) pharmacokinetic (PK) model, expressed using linear ordinary differential equations (ODEs), to describe the molecular concentrations following a single IVT injection. The model was fit to experimental rabbit data, with Fab, Fc, IgG and IgG null antibodies and antibody fragments, to estimate key ocular pharmacokinetic parameters. The model predicts an ocular half-life,  $t_{1/2}$ , which is the same for all compartments and dependent on the hydrodynamic radius ( $R_h$ ) of the respective molecules, consistent with observations from the experimental data. Estimates of the permeabilities of the RPE and ILM are derived for  $R_h$  values ranging from 2.5 to 4.9 nm, and are found to be in good agreement with ex-vivo measurements from bovine eyes. We show that the ratio of these permeabilities largely determines the ratio of the molecular concentrations in the retina and vitreal compartments and their dependence on  $R_h$ . The model further provides estimates for

the ratio of fluxes corresponding to the elimination pathways from the eye, i.e., aqueous humor to retina/choroid, which increase from 5:1 to 7:1 as  $R_h$  decreases. Our semi-mechanistic model provides a quantitative framework for interpreting ocular PK and the effects of molecule size on rate-determining parameters. We have shown that intra-ocular permeabilities can be reasonably estimated from 3-compartment ocular PK data and determined how these parameters influence the half-life, retinal permeation and elimination of intravitreally injected molecules from the eye.

#### Keywords

Retina; Permeability; Intravitreal; Pharmacokinetics; Mechanistic modelling.

## Introduction

Therapeutic antibodies and antibody fragments, administered via intravitreal (IVT) injection, are successfully used to treat retinal diseases, such as neovascular age-related macular degeneration (wet AMD) and diabetic macular edema. It is assumed that such molecules should be able to penetrate the retina in order to achieve maximum efficacy<sup>1</sup>. The elimination of drugs given by IVT injection primarily occurs by diffusion from the vitreous chamber into the aqueous humor; transport also occurs between the vitreous and retina, and between the retina and choroid, which provides a second ocular elimination pathway<sup>2,3</sup>. The inner limiting membrane (ILM) of the retina, separating it from the vitreous, acts as a biological barrier, impeding macromolecular drug diffusion into the retina. Due to this barrier, and the vitreous-aqueous elimination pathway, much of a drug delivered via IVT injection does not reach the retina. Certain retinal diseases, such as wet AMD, may require subretinal drug permeation, through the retinal pigment epithelium (RPE) and into the choroid. The RPE itself acts as a tight biological barrier - in a similar manner to the ILM, as well as being a major part of the blood-retinal barrier (BRB)<sup>4</sup>, we seek to mechanistically describe and quantify the impact of these phenomena on drug availability within the retina.

In order to improve the properties of IVT-injected drugs, it is crucial to quantitatively understand the pathways and barriers described above. Understanding the influence of molecular size on these processes is also essential in antibody drug design, as well as for potential gene therapies that utilize large adeno-associated virus (AAV) particles to encapsulate the drug<sup>5</sup>. In the present work we extend our previous 2-compartment model (vitreous chamber and aqueous humor) of IVT pharmacokinetics<sup>6</sup> by adding a retinal compartment and incorporating the intraocular transport pathways between vitreous, retina and choroid, and the associated ILM and RPE barriers described above.

Building upon the 2-compartment model<sup>6</sup>, we present a semi-mechanistic 3-compartment PK mathematical model, describing the molecular concentration over time in the retina, vitreous and aqueous, following a single IVT injection. We retain the PK aspects of the 2-compartment PK/PD ordinary differential equation (ODE) model in Hutton-Smith et. al.<sup>6</sup>, while extending it to include retinal PK. We calibrate our semi-mechanistic 3-compartment IVT PK model using the experimental data obtained by Gadkar et. al.<sup>7</sup> in the rabbit with IgG, IgG null, Fc and Fab fragments. These datasets exhibit a common ocular half-life ( $t_{1/2}$ ) in the retina, vitreous and aqueous compartments whose value depends on the hydrodynamic radius of the molecule ( $R_h$ ). Our model provides a mechanistic basis for this finding and further enables us to derive estimates of the permeability coefficients of the ILM and RPE and their apparent dependence on  $R_h$ , which we compare to experimental values from the literature<sup>8</sup>.

Utilizing the analytic solution to the ODE system we provide key pharmacological metrics, such as  $t_{1/2}$ , in terms of physiological parameters, and comment on how they differ from the standard 2-compartment model. Lastly we use the model to estimate the ratio of the ocular elimination from the aqueous humor to the ocular elimination from the retina/choroid as a function of molecular size.

A recent review of the pharmacokinetic aspects of retinal drug delivery, del Amo et al.<sup>9</sup>, describes the various biological barriers within the retina and the difficulty of achieving clinically efficacious drug concentrations there. It further emphasizes the utility of PK models to address this issue and suggests that future models should include descriptions of the retinal tissue itself, as well as the surrounding membranes. We believe that the present 3-compartment mechanistic model, incorporating the permeabilities of the ILM and RPE, is an important step in this direction.

## Methods

### Experimental data

We utilized data from a recently published study by Gadkar et. al.<sup>7</sup> provided by these authors, detailing the concentration-time profiles in the retina, vitreous and aqueous, for a number of antibodies and antibody fragments, following IVT injection. The study was performed in rabbits using molecules derived from a human anti-glycoprotein D (anti-gD) antibody, and hence inert in a rabbit model, forgoing the need to account for pharmacodynamic (PD) effects. The particular datasets analyzed in this study were for Fab, Fc, IgG and IgG null molecules (noting that IgG null molecules are IgG molecules with fragment crystallizable (Fc) region mutations that prevent binding to neonatal Fc receptor (FcRn)), whose respective parameter values can be found in Table 1. Retinal, vitreous and aqueous antibody concentrations were measured at 0.25, 2, 8, 14,

21 and 28 days, excluding the Fc dataset wherein only vitreous and aqueous data were available. The Fab dataset contains retinal data not reported as part of the original study<sup>7</sup>, but provided as an additional dataset by Gadkar et. al. and Genentech (for details of this dataset, as well as others mentioned see Section 1 of the supporting information for all experimental datasets utilized in this study).

Table 1: Summary of biophysical properties of antibody and antibody fragments. Weights and doses taken from Gadkar et. al.<sup>7</sup>, hydrodynamic radii ( $R_h$ ) taken from Shatz 2016 et. al.<sup>10</sup>, specifically the values reported for G10rabFab and G10rabIgG molecules. \*Doses correspond to experimental protocol except for IgG null which was estimated from initial vitreous concentrations assuming a vitreal volume of 1.52 mL (Table 2).

Antibody	Molecular weight (kDa)	Hydrodynamic radius (nm)	Initial dose (mg)*
Fab	50	2.5	0.615
Fc	50	2.5	0.5
IgG	150	4.9	0.549
IgG null	150	4.9	0.75

### Model description

The 3-compartment model, described graphically in Figure 1, is comprised of the retina, vitreous and aqueous chambers, with respective antibody concentrations  $c_{\text{ret}}(t)$ ,  $c_{\text{vit}}(t)$  and  $c_{\text{aq}}(t)$ , in pM. An initial IVT injection is administered at  $t = 0$ , resulting in an initial vitreal concentration of  $c_0$  pM. The drug at this point is free to move from the vitreous into the aqueous and retina, as well as back from the retina into the vitreous. The drug is cleared from the aqueous humor compartment at a rate corresponding to the aqueous humor production (mL/day), and is eliminated from the retina, via the RPE, into the choroid (assumed to be a sink). After elimination from the aqueous compartment or choroid, the drug enters the systemic circulation where it is eventually cleared from the body; recirculation to the eye is assumed to be negligible. All transport pathways are taken to be first order, and are indicated in Figure 1 by arrows with their respective transport rates, given in terms of the parameters in Table 2. As we formulated this model in terms of concentration, all mechanistic transport rates have volume factors to account for compartment size (as shown in Figure 1). Note the difference in transfer rate between the retina and vitreous, dependent on direction. The model is then formulated as a system of linear ODEs, given by Equations 1-3, with initial conditions  $c_{\text{vit}}(0) = c_0$  and  $c_{\text{ret}}(0) = c_{\text{aq}}(0) = 0$ :

$$\frac{dc_{\text{ret}}}{dt} = -\left(\frac{S_{\text{ret}}}{V_{\text{ret}}}\right) [p_{\text{ILM}} + p_{\text{RPE}}] c_{\text{ret}} + \left(\frac{S_{\text{ret}}}{V_{\text{ret}}}\right) p_{\text{ILM}} c_{\text{vit}}, \quad (1)$$

$$\frac{dc_{\text{vit}}}{dt} = \left(\frac{S_{\text{ret}}}{V_{\text{vit}}}\right) p_{\text{ILM}} c_{\text{ret}} - \left[ \left(\frac{S_{\text{ret}}}{V_{\text{vit}}}\right) p_{\text{ILM}} + k_{\text{el}} \right] c_{\text{vit}}, \quad (2)$$

$$\frac{dc_{\text{aq}}}{dt} = \left(\frac{V_{\text{vit}}}{V_{\text{aq}}}\right) k_{\text{el}} c_{\text{vit}} - \left(\frac{CL_{\text{aq}}}{V_{\text{aq}}}\right) c_{\text{aq}}. \quad (3)$$

An alternative formulation of Equations 1-3 can be found in Section 3 of the supporting information, which explains in greater detail how Figure 1 translates into this system of ODEs. The analytic solution of Equations 1-3 can be found in Section 4 of the supporting information, wherein all three compartments were found to decay at the same rate (post transient behaviour). The original study<sup>7</sup> introduced a phenomenological delay compartment separating the vitreous and aqueous compartments, via first order transport processes. For simplicity we have omitted this delay process in the analysis presented here as it only affects the initial aqueous compartment data points and does not influence significantly aspects of model behavior in which we are interested (see Section 5 in the supporting information for analysis that includes the delay compartment).

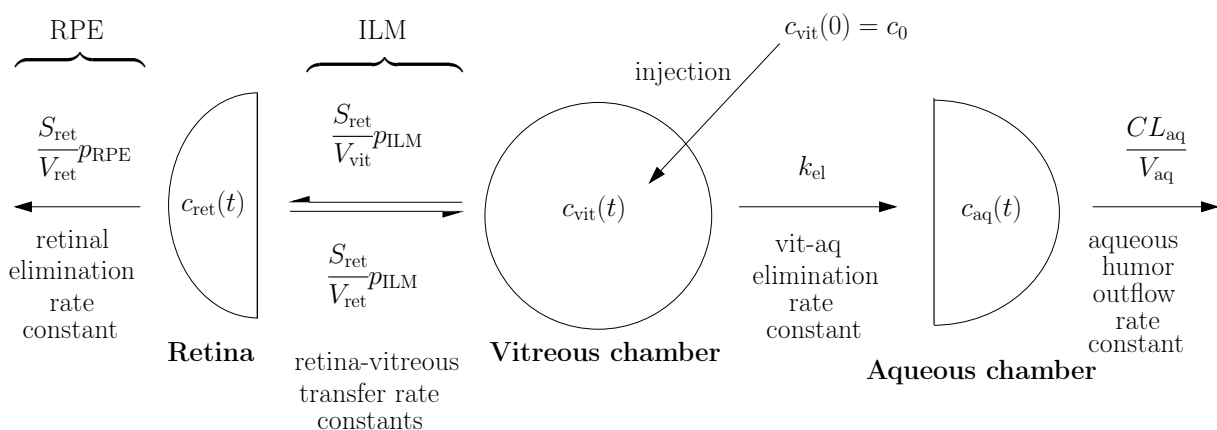


Figure 1: 3-compartment PK model for a general antibody, following a single IVT injection. Transport pathways are indicated by arrows, with their respective transfer rate constants. The antibody concentrations in the retina, vitreous and aqueous are denoted, respectively, as  $c_{\text{ret}}(t)$ ,  $c_{\text{vit}}(t)$  and  $c_{\text{aq}}(t)$ . Overbraces indicate the retinal pigment epithelium, RPE, and the inner limiting membrane, ILM, situated between the posterior and anterior of the retina, respectively.

Table 2: Summary of model parameters, units and notation. \*Derivations for the values of  $V_{\text{ret}}$  and  $S_{\text{ret}}$  can be found in Section 2 of the supporting information. Estimated parameters were treated as free during the fitting protocol and were approximated from experimental datasets for each molecule studied.

Parameter	Value	Units	Description
$p_{\text{RPE}}$	Estimated	cm/sec	Permeability of the retinal pigment epithelium (RPE)
$p_{\text{ILM}}$	Estimated	cm/sec	Permeability of the inner limiting member of the retina (ILM)
$k_{\text{el}}$	Estimated	1/day	Elimination from the vitreous to aqueous chamber
$CL_{\text{aq}}$	4.32 <sup>11,12</sup>	ml/day	Clearance from the aqueous chamber
$V_{\text{ret}}$	0.044*	ml	Retinal volume
$V_{\text{vit}}$	1.52 <sup>12</sup>	ml	Vitreous volume
$V_{\text{aq}}$	0.325 <sup>12</sup>	ml	Aqueous volume
$S_{\text{ret}}$	4.35*	cm <sup>2</sup>	Retinal surface area

### Fitting protocol

When fitting the model to the experimental data,  $p_{\text{RPE}}$ ,  $p_{\text{ILM}}$  and  $k_{\text{el}}$  were allowed to be varied by the fitting algorithm, with all other parameters fixed at their values given in Table 2. Initial data points in the aqueous humor, at time 0.25 days, were omitted (see Section 5 of the supporting information for justification).

The free parameters were optimized by penalizing the relative mean-square error (MSE) between the logarithmic values of model results and the data, using `lsqnonlin`<sup>13</sup> (part of MATLAB’s optimization toolbox). Confidence intervals were generated using a bootstrap algorithm with re-sampling<sup>14,15</sup>.

## Results

Figure 2 shows optimized fits for the retina, vitreous and aqueous datasets from Gadkar et. al.<sup>7</sup> (see Section 6 of the supporting information to view these fits plotted individually by molecule). Best fit parameters and confidence intervals can be found in Table 3, and their dependence on  $R_h$  is illustrated in Figure 3. Figure 2 demonstrates the model’s ability to fit to the data, with a common half-life across compartments that is molecule specific. Figure 3, in conjunction with Table 3, shows that the estimated values of all elimination rate determining parameters ( $p_{RPE}$ ,  $p_{ILM}$ ,  $k_{el}$ ) are higher for molecules of smaller hydrodynamic radius ( $R_h$ ), contributing to a shorter half life ( $t_{1/2}$ ) value.

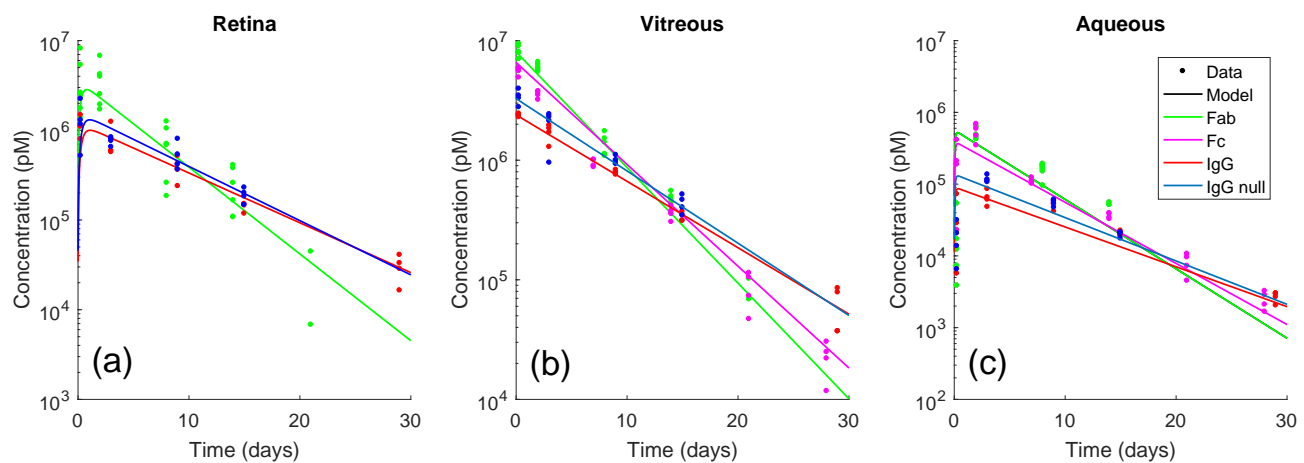


Figure 2: Compilation of optimized fits to the dataset<sup>7</sup>. Colored markers indicate distinct molecule datasets, whereas colored lines show the optimized fit. For Fc molecules there was no retina data available, only vitreous and aqueous humor concentrations. See Section 6 of the supporting information to view these fits plotted by molecule.

Table 3: Best fit parameter summary, including 95% confidence intervals obtained via Monte Carlo simulations using error bootstrapping<sup>14</sup>. Due to the lack of retinal data for molecule Fc, estimates for  $p_{RPE}$  and  $p_{ILM}$  could not be obtained in this case. RMSE, the root mean square error, is taken between the data and the model best fit.

Parameter	Best fit parameter value (95% confidence interval)				Units
	Fab	Fc	IgG	IgG null	
$p_{RPE}$	2.60 (1.36, 4.04)	n/a	1.84 (1.08, 2.36)	1.91 (1.07, 2.5)	$\times 10^{-7}$ cm/sec
$p_{ILM}$	1.88 (1.13, 2.81)	n/a	1.7 (0.912, 2.32)	1.65 (7.58, 2.52)	$\times 10^{-7}$ cm/sec
$p_{RPE}/p_{ILM}$	1.38 (0.707, 2.21)	n/a	1.08 (0.612, 1.57)	1.16 (0.655, 1.64)	none
$k_{el}$	0.197 (0.179, 0.219)	0.169 (0.161, 0.178)	0.107 (0.0985, 0.119)	0.118 (0.109, 0.131)	1/day
$t_{1/2}$	3.11	3.54	5.42	4.98	days
RMSE	11.4	4.2	1.8	3.4	$\times 10^5$ pM

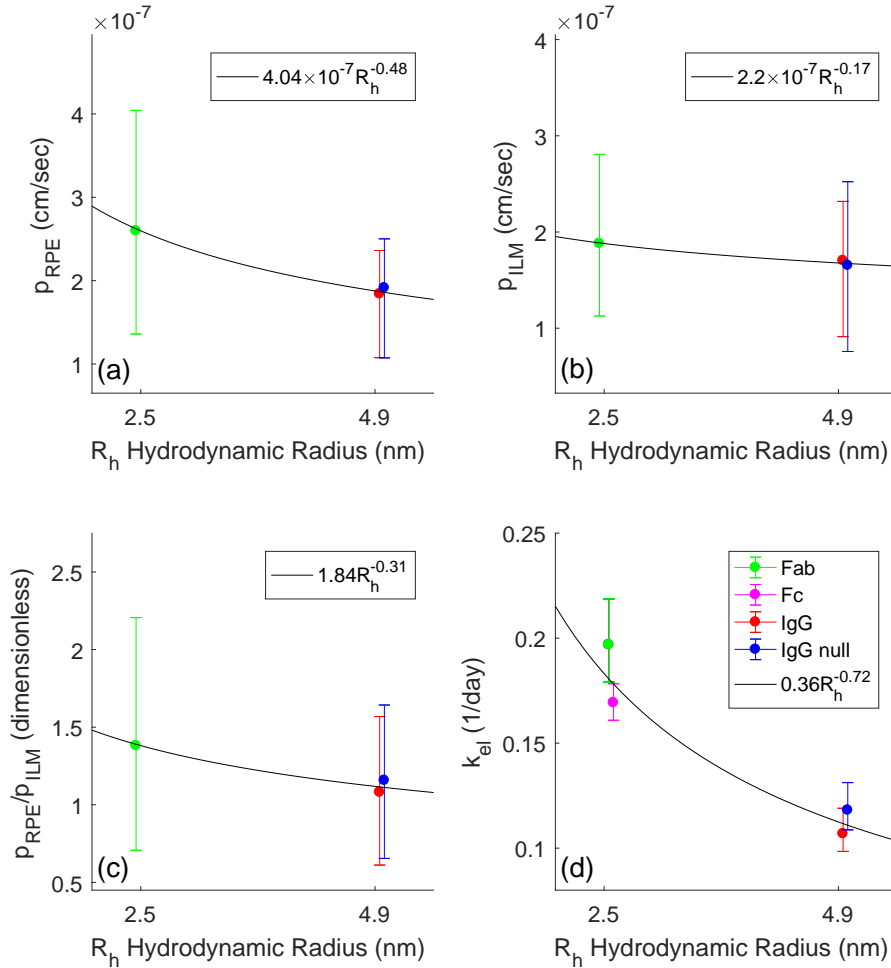


Figure 3: Best fit parameters plotted with respect to hydrodynamic radius ( $R_h$ ). Error bars represent 95% confidence intervals obtained via Monte Carlo simulations using error bootstrapping<sup>14</sup>. Power law fits, with respect to  $R_h$ , are shown by the solid lines, the equations of which are given in each subplot's legend.  $R_h$  values for Fab, IgG and IgG null molecules were taken from<sup>10</sup>. Power laws were chosen here as a means to interpret within the region of interest.

#### Comparison of estimated permeabilities to experimental data

In Figure 4 we present comparisons of our estimations for  $p_{RPE}$  with a 2005 study by Pitkanen et al.<sup>8</sup> which analyzed the permeability of the RPE, in bovine eyes, to molecules with  $R_h$  ranging from 1.3 to 6.4 nm.<sup>8</sup> The model derived estimates for  $p_{RPE}$  (green, red and blue) fit well within the experimentally derived range of RPE permeabilities, occupied by the molecules of similar  $R_h$ . The solid black curve in Figure 4 is a power law, fit to all data points shown.

A 2014 study by Vacca et al. suggests the ILM of the wild type mouse is relatively impermeable to adeno-associated virus 5 (AAV5) nanoparticles compared to the retina of mice lacking the Dp71 gene.<sup>16</sup> The minimum  $R_h$  for monomeric AAVs is approximately 14 nm<sup>17</sup>. The power law predicted from the combination of our estimations and the dataset in Pitkanen et. al.<sup>8</sup>, predicts an upper bound of the permeability of virus particles at approximately  $3.05 \times 10^{-8}$  cm/sec. This value is an order of magnitude smaller when compared to our estimates for full and fragment antibodies.

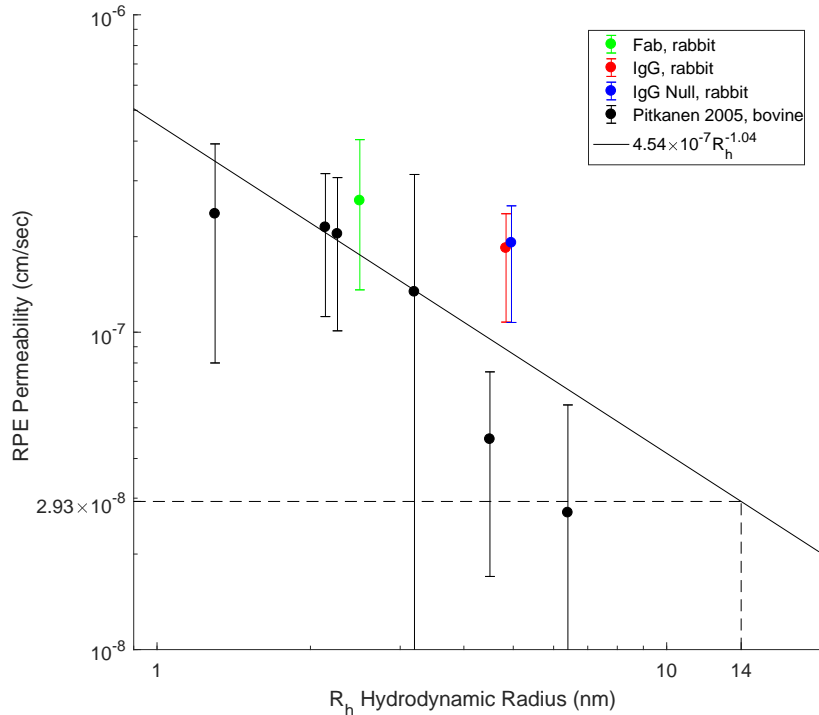


Figure 4: Comparison between full experimental bovine dataset<sup>8</sup> and best fit values for RPE permeability, found in Table 3. The solid black line denotes a power law fit to these data points, whose parameters, magnitude and exponent (with 95% confidence intervals), are  $4.54 \times 10^{-7}$  ( $1.24 \times 10^{-7}$ ,  $16.6 \times 10^{-7}$ ) and  $-1.04$  ( $-2.07$ ,  $-0.01$ ), respectively. The dashed lines denote the expected permeability (as predicted by the power law) of molecules with hydrodynamic radius of 14 nm.

#### Vitreous retina concentration ratio and $t_{12}$ expressions

The vitreous retina ratio is defined as  $R_{VR}(t) = c_{vit}(t)/c_{ret}(t)$ , and the analysis in Section 7 of the supporting information shows, post initial chemical equilibration, that this expression is constant and given approximately by:

$$R_{VR} \simeq 1 + \frac{p_{RPE}}{p_{ILM}}. \quad (4)$$

This equation demonstrates that as  $p_{RPE}$  tends to zero, with  $p_{ILM}$  held constant, the vitreous and retina approximately equilibrate to the same concentration. Our fitting protocol suggests that the value of  $p_{RPE}/p_{ILM}$  lies in the range of 1.1-1.4 (Figure 3C), implying the antibody concentration of the vitreous is roughly double that of the retina at any given time. Section 7 of the supporting information also presents an analytic approximation for the long time decay rate,  $\lambda_1$ ,

$$\lambda_1 \simeq k_{el} + \left( \frac{S_{ret} p_{ILM}}{V_{vit}} \right) - \frac{1}{1 + \frac{p_{RPE}}{p_{ILM}}} \left( \frac{S_{ret} p_{ILM}}{V_{vit}} \right) \quad (5)$$

$$= k_{el} + \frac{S_{ret}}{V_{vit}} \left( \frac{1}{\frac{1}{p_{RPE}} + \frac{1}{p_{ILM}}} \right), \quad (6)$$

where we note that  $\lambda_1$  is related to the half life ( $t_{1/2}$ ) via the following expression:

$$t_{1/2} = \frac{\log 2}{\lambda_1}. \quad (7)$$



In previous 2-compartment models<sup>6,18</sup> the decay rate is equal to  $k_{\text{el}}$ , as can be seen in Equation 5 by setting  $p_{\text{ILM}}$  equal to zero (effectively reducing the model in Figure 1 to a 2-compartment model). Notably this is also the case when  $p_{\text{RPE}}$  is set to zero, as in this limit the vitreous and retina become indistinguishable (see Figure 1), i.e. in a state of quasi equilibrium, where there is no retinal elimination. The second term on the right-hand side of Equation 5 shows us the effect of allowing an additional transport pathway from the vitreous chamber, through the ILM and into the retina; this term simply increases the decay rate equal to the rates of transfer through the ILM. The third term on the right-hand side of Equation 5 describes, in a simple analytic expression, the complex interplay between the vitreous and retina, and arises due to the bi-directional transport between these 2 compartments. This term acts as a damping term, reducing the decay rate, as molecules which permeate into the retina are then able to return to the main body of the eye. We see that this term is inversely proportional to the vitreous to retina concentration ratio, implying that the bi-directional nature of transport across the ILM dampens the additional decay caused by choroidal elimination by approximately half. Equation 6 demonstrates the symmetrical influence of  $p_{\text{ILM}}$  and  $p_{\text{RPE}}$  on  $\lambda_1$  in the limiting cases when either term tends to zero (yielding  $k_{\text{el}}$ ) or infinity (yielding  $k_{\text{el}} + (S_{\text{ret}}/V_{\text{vit}}) \times p_{\text{ILM}}$  or  $p_{\text{RPE}}$ ). Notice also the similarity between the second term in Equation 6 and the total resistance of two resistors in series, if the reciprocal of permeability is taken as analogous to electrical resistance.

#### Aqueous to retinal elimination ratio

Following IVT injection, the approximate number of molecules (given in pmols), over all time, which exit via the RPE and via the aqueous are given, respectively, by  $E_{\text{RPE}}$  and  $E_{\text{aq}}$ . The ratio,  $E_{\text{aq}}/E_{\text{RPE}}$ , is shown in Section 8 of the supporting information to be approximately described by:

$$\frac{E_{\text{aq}}}{E_{\text{RPE}}} \simeq \frac{k_{\text{el}} V_{\text{vit}}}{S_{\text{ret}}} \left( \frac{1}{p_{\text{RPE}}} + \frac{1}{p_{\text{ILM}}} \right). \quad (8)$$

Table 4 contains this expression evaluated for Fab, IgG and IgG null molecules, showing that for each IVT-injected antibody that passes through the RPE into the choroid, 5-7 antibody molecules will be eliminated via the aqueous humor. This reinforces the assumption made in previous models<sup>6,7</sup> that the aqueous humor is the critical transport pathway within the model, justifying the neglect of elimination via the RPE.

Table 4: The aqueous to retinal elimination ratio,  $E_{\text{aq}}/E_{\text{RPE}}$ , is the ratio of the number of molecules that left the system via the aqueous and the number that left through the RPE, post transient chemical equilibration. Section 8 of the supporting information details the calculations of these values.

Molecule	Fab	IgG	IgG null
Percentage of dose exiting through RPE	12.7%	17.6%	16.3%
Percentage of dose exiting through aqueous	87.3%	82.4%	83.7%
$E_{\text{aq}}/E_{\text{RPE}}$	6.87	4.68	5.14

## Discussion

In contrast to the original model used to analyze these data,<sup>7</sup> our semi-mechanistic approach models the membranes on either side of the retina in terms of their permeabilities ( $p_{\text{ILM}}$  and  $p_{\text{RPE}}$ ), incorporating transport between the vitreous and retina, as well as choroidal elimination. This allows for geometric scaling of this model across species (via adjustment of volumes and surface areas) to, for example, humans, granting applicability of our model to a wider range of experimental and clinical data. Due to the semi-mechanistic nature of our model, the derived half life ( $t_{1/2}$ ) given by Equations 5-7 also scales geometrically, giving a valuable physiological relationship that is translatable across species. In this regard our model predicts (rather than assumes) that a common value of  $t_{1/2}$  describes the time-course of drug concentration in the aqueous, vitreous and retina compartments.

While all three compartments exhibit the same apparent  $t_{1/2}$  (derived from  $\lambda_1$ ), we note that the aqueous and retinal compartments exhibit the pharmacokinetic "flip-flop" phenomenon in comparison to the vitreous compartment. This phenomenon occurs when the rate constant of drug input to a compartment is smaller than the rate constant of drug elimination<sup>19</sup>. In the aqueous compartment, the rate constant of drug input from the vitreous ( $k_{\text{el}}$ ) is comparable to  $\lambda_1$ , which is on the order of 0.1 to 0.2 day<sup>-1</sup>, and is much smaller than the elimination rate constant from the aqueous compartment ( $CL_{\text{aq}}/V_{\text{aq}} = 13.3$  day<sup>-1</sup>). In the retina the rate constant of drug input from the vitreous also reflects  $\lambda_1$  and is smaller than the elimination rate constant from the retina ( $p_{\text{RPE}}S_{\text{ret}}/V_{\text{ret}}$ ) which is on the order of 2 day<sup>-1</sup>.

We have shown that the model can be used to estimate permeabilities from 3-compartment PK data, and observe a similar magnitude and trend in our estimated permeability values with  $R_{\text{h}}$  as seen in bovine retina by Pitkanen et al.<sup>8</sup>. Additionally we note our RPE permeability estimates agree with the predicted values of retina to choroid permeability, generated from a model of the blood-retinal barrier (BRB)<sup>4</sup>. In Tervonen et. al.<sup>4</sup> molecules with radii in the range of 0.5-0.9 nm were studied, those with a  $R_{\text{h}}$  value of 0.9 nm were predicted to have a retina to choroid permeability of approximately  $5 \times 10^{-7}$  cm/sec, which is in broad agreement with the power law

fit to data in Figure 4.

Our estimates of the ILM and RPE permeabilities as well as their ratio (Table 3), suggest  $p_{\text{ILM}}$  and  $p_{\text{RPE}}$  are comparable in magnitude and vary weakly with  $R_h$ . From the structural perspective, the ILM and RPE barriers are both composed of basement membranes containing laminins, proteoglycans and collagens (Halfter et al.<sup>20</sup>) and an adherent cellular layer. In the ILM the cellular layer corresponds to the foot processes of the Muller cells; while in the RPE it is the pigmented epithelial cells, which form tight junctions between them. In both cases the cellular layers are anchored to the basement membrane by laminin proteins (see Vacca et. al.<sup>16</sup>). Recent in vitro studies suggest that basement membranes may contribute to the macromolecular barrier properties of epithelia (Vllasaliu et. al.<sup>21</sup>). Transcellular and paracellular pathways also appear to contribute to the permeability of the RPE for Ranibizumab (Fab) and Bevacizumab (IgG) (Terasaki et. al.<sup>22</sup>). Direct measurements of  $p_{\text{ILM}}$  and  $p_{\text{RPE}}$  and their components, e.g., basement membranes and cellular layers, are needed to further assess the contribution of these layers as well as the influence of macromolecular size, structure and charge on the respective permeabilities.

Due to the limited available data and uncertainty in our estimated permeabilities for the ILM and RPE we caution against extrapolating the permeability power relations shown in Figure 3 much beyond their respective range of  $R_h$  values. Although the extrapolated estimate of  $p_{\text{RPE}}$  for the 14 nm AAV particles is consistent with studies in the mouse<sup>16</sup>, further experimental data over a range of macromolecular sizes and chemical properties (including charge density) are needed to better define the dependences of  $p_{\text{RPE}}$ ,  $p_{\text{ILM}}$  and  $k_{\text{el}}$  on  $R_h$ . In this regard, we have shown how the 3-compartment PK model can be used to estimate such physiological parameters from ocular PK data obtained in the aqueous, vitreous and retinal compartments.

While acknowledging the limited data available to define the dependence of the parameter  $k_{\text{el}}$  on  $R_h$  (Figure 3d), we note that it is approximately proportional to  $1/R_h$ ; a result that is consistent with our previous conjecture<sup>6</sup>. For sufficiently small  $p_{\text{ILM}}$  (as occurs in the rabbit), Eqs. 5-7 imply that the ocular half-life ( $t_{1/2}$ ) will be approximately equal to  $1/k_{\text{el}}$  and thus  $t_{1/2}$  should increase with  $R_h$ . Shatz et al.<sup>10</sup> have recently confirmed such a relationship in the rabbit using pegylated Fab molecules with  $R_h$  ranging from 2.5 to 6.9 nm. Further development of the theoretical factors that determine  $k_{\text{el}}$  would be useful for translating the data from rabbits to other species<sup>6</sup>.

The analytic approximation for the decay rate  $\lambda_1$  (Equation 5) shows how the retinal elimination pathway and bidirectional transport across the ILM impact  $\lambda_1$  and, hence,  $t_{1/2}$  (Equation 7). In

comparison to the previous 2-compartment models<sup>6,18</sup> (where  $\lambda_1$  is equal to  $k_{el}$ ), the additional terms contribute about 11-16% to  $\lambda_1$  and lead to a similar reduction in the estimated value of  $k_{el}$  as that obtained from the 2-compartment model. We further note that the ratio of the retinal permeabilities,  $p_{RPE}/p_{ILM}$ , appears in long time decay rate (Equation 5), the vitreous-to-retina concentration ratio (Equation 4) and the aqueous-to-retinal elimination ratio (Equation 8). This ratio results from the bidirectional transport between the vitreous and retina and is a key factor that determines the ocular pharmacokinetics associated with intravitreal administration. Direct measurements of the permeabilities of the ILM and the RPE would be useful to confirm the estimates obtained from the semi-mechanistic PK model.

The recent review of the pharmacokinetic aspects of retinal drug delivery, del Amo et. al.<sup>9</sup>, presented a metadata analysis of intravitreal elimination rates over a wide range of molecules. Using the data presented by Pitkanen et. al.<sup>8</sup> the authors concluded that 3-20% of the injected dose is eliminated through the RPE, we find this to be consistent with our results, given in Table 4, which state that our model predicts 13-18% of molecules studied exit via the RPE. Our analysis also shows that the magnitude of the aqueous to retinal elimination ratio, Equation 8, yields the counter-intuitive finding that molecules with a larger  $R_h$  value are eliminated at a higher rate through the choroid than molecules with lower  $R_h$  values. Equation 8 tells us that the ratio of the number of molecules eliminated through the aqueous as opposed to the choroid is dependent on  $k_{el}$ ,  $p_{RPE}$  and  $p_{ILM}$ . Our parameter estimation across molecular species indicates that the magnitude of  $k_{el}$  is more sensitive to a change in  $R_h$  than  $p_{RPE}$  and  $p_{ILM}$ , which were found to be relatively insensitive. We therefore find that due to the notable drop in the magnitude of  $k_{el}$  between Fab and IgG molecules (by approximately 50%), simulated IgG molecules were retained longer within the vitreous, and were hence eliminated at a higher rate through the choroid relative to Fab molecules. Increasing the number of molecules eliminated via the choroid relative to the aqueous is potentially advantageous from the perspective of drug delivery for many ocular antibodies, which target the posterior of the retina in the treatment of retinal diseases. We note that due to the magnitude of the confidence intervals for model permeabilities, we suggest that further data are required to confirm that  $k_{el}$  is significantly more sensitive to  $R_h$  than  $p_{RPE}$  and  $p_{ILM}$ , and suggest permeability studies of the RPE and ILM in tandem.

Both retinal, vitreal and aqueous PK data are required in order to estimate retinal permeabilities, however very few such datasets currently exist. In order to more accurately describe the dependence of  $p_{ILM}$ ,  $p_{RPE}$  and  $k_{el}$  on  $R_h$ , data over a wider range of hydrodynamic radii are required. With such information our semi-mechanistic model will yield better predictions regarding the effects of molecular size on retinal concentration and choroidal

elimination. This 3-compartment PK model can also be straightforwardly extended into a PK/PD model, through the inclusion of reaction kinetics, and then used to analyze clinical data. As in Hutton-Smith et. al.<sup>6</sup>, such a PK/PD model could be used to study ranibizumab binding to vascular endothelial growth factor (VEGF) in the eye. In principle such a model could be used to infer the kinetics of VEGF suppression in the retina, based on the observed suppression of VEGF levels in the aqueous humor.

## Supporting Information

1. Antibody and Antibody Fragment PK datasets, 2. Rabbit retinal geometric parameter derivations, 3. Model Equations Conversion from pM to fmol, 4. Model Solution, 5. Delay model, 6. Non-delay model individual plots, 7. Half life and Vitreous Retina Ratio Analytic Approximation, 8. RPE-Aqueous elimination ratio.

## Acknowledgements

Funding provided to Wolfson Centre of Mathematical Biology by EPSRC and MRC (Grant No. EP/L016044/1). Additional funding provided by Roche Pharma Research and Early Development.

## References

- (1) Ranta, V. P.; Mannermaa, E.; Lummeppuro, K.; Subrizi, A.; Laukkanen, A.; Antopolsky, M.; Murtomäki, L.; Hornof, M.; Urtti, A. Barrier analysis of periocular drug delivery to the posterior segment. *Journal of Controlled Release* **2010**, *148*, 42–48.
- (2) Gaudana, R.; Ananthula, H. K.; Parenky, A.; Mitra, A. K. Ocular drug delivery. *The AAPS journal* **2010**, *12*, 348–360.
- (3) Maurice, D. M. Protein Dynamics in the Eye Studied with Labelled Proteins. *American Journal of Ophthalmology* **1959**, *47*, 361–368.
- (4) Tervonen, A.; Vainio, I.; Nymark, S.; Hyttinen, J. Prediction of passive drug permeability across the blood-retinal barrier. *Pharmaceutical Research* **2014**, 1–15.
- (5) Boye, S. E.; Boye, S. L.; Lewin, A. S.; Hauswirth, W. W. A comprehensive review of retinal gene therapy. *Molecular Therapy* **2013**, *21*, 509–519.
- (6) Hutton-Smith, L. A.; Gaffney, E. A.; Byrne, H. M.; Maini, P. K.; Schwab, D.; Mazer, N. A. A mechanistic model of the intravitreal pharmacokinetics of large molecules and the pharmacodynamic suppression of ocular VEGF levels by ranibizumab in patients with

neovascular age-related macular degeneration. *Molecular pharmaceuticals* **2016**, *13*, 2941–2950.

- (7) Gadkar, K. et al. Design and Pharmacokinetic Characterization of Novel Antibody Formats for Ocular Therapeutics. *Investigative Ophthalmology & Visual Science* **2015**, *56*, 5390–5400.
- (8) Pitkänen, L.; Ranta, V. P.; Moilanen, H.; Urtti, A. Permeability of retinal pigment epithelium: Effects of permeant molecular weight and lipophilicity. *Investigative Ophthalmology and Visual Science* **2005**, *46*, 641–646.
- (9) del Amo, E. M. et al. Progress in Retinal and Eye Research Pharmacokinetic aspects of retinal drug delivery. *Progress in Retinal and Eye Research* **2016**, *12*.
- (10) Shatz, W.; Hass, P. E.; Mathieu, M.; Kim, H. S.; Leach, K.; Zhou, M.; Crawford, Y.; Shen, A.; Wang, K.; Chang, D. P.; Maia, M.; Crowell, S. R.; Dickmann, L.; Scheer, J. M.; Kelley, R. F. Contribution of Antibody Hydrodynamic Size to Vitreal Clearance Revealed through Rabbit Studies Using a Species-Matched Fab. *Molecular Pharmaceuticals* **2016**, *13*, 2996–3003.
- (11) Bárány, E.; Kinsey, V. E. The Rate of Flow of Aqueous Humor. *American Journal of Ophthalmology* **1949**, *32*, 177–188.
- (12) Missel, P. J. Simulating intravitreal injections in anatomically accurate models for rabbit, monkey, and human eyes. *Pharmaceutical Research* **2012**, *29*, 3251–3272.
- (13) The MathWorks Inc, MATLAB user guide R2015b: Global Optimization Toolbox, 2015. 2015.
- (14) Motulsky, H.; Christopoulos, A. Fitting models to biological data using linear and nonlinear regression. *PRISM Manual* **2003**,
- (15) Efron, B.; Tibshirani, R. *An Introduction to the Bootstrap*; Chapman & Hall, 1994.
- (16) Vacca, O.; Darche, M.; Schaffer, D. V.; Flannery, J. G.; Sahel, J. A.; Rendon, A.; Dalkara, D. AAV-mediated gene delivery in Dp71-null mouse model with compromised barriers. *Glia* **2014**, *62*, 468–476.
- (17) Wright, J. F.; Le, T.; Prado, J.; Bahr-Davidson, J.; Smith, P. H.; Zhen, Z.; Sommer, J. M.; Pierce, G. F.; Qu, G. Identification of factors that contribute to recombinant AAV2 particle aggregation and methods to prevent its occurrence during vector purification and formulation. *Molecular Therapy* **2005**, *12*, 171–178.
- (18) Saunders, D. J.; Muether, P. S.; Fauser, S. A model of the ocular pharmacokinetics involved in the therapy of neovascular age-related macular degeneration with ranibizumab. *British Journal of Ophthalmology* **2015**, 1–6.

- (19) Yáñez, J. A.; Remsberg, C. M.; Sayre, C. L.; Forrest, M. L.; Neal, M. challenges and opportunities during drug development. **2012**, *2*, 643–672.
- (20) Halfter, W.; Dong, S.; Dong, a.; Eller, a. W.; Nischt, R. Origin and turnover of ECM proteins from the inner limiting membrane and vitreous body. *Eye (London, England)* **2008**, *22*, 1207–1213.
- (21) Vllasaliu, D.; Falcone, F. H.; Stolnik, S.; Garnett, M. Basement membrane influences intestinal epithelial cell growth and presents a barrier to the movement of macromolecules. *Experimental Cell Research* **2014**, *323*, 218–231.
- (22) Terasaki, H.; Sakamoto, T.; Shirasawa, M.; Yoshihara, N.; Otsuka, H.; Sonoda, S.; Hisatomi, T.; Ishibashi, T. Penetration of Bevacizumab and Ranibizumab Through Retinal Pigment Epithelial Layer in Vitro. *Retina* **2015**, *35*, 1007–1015.

---

# Supporting Information

**For paper entitled:** Ocular Pharmacokinetics of Therapeutic Antibodies Given by Intravitreal Injection:  
Estimation of Retinal Permeabilities Using a 3-Compartment Semi-Mechanistic Model

---

Laurence A. Hutton-Smith, Eamonn A. Gaffney, Helen M. Byrne,  
Philip K. Maini, Kapil Gadkar, Norman A. Mazer

## CONTENTS

1	Antibody and Antibody Fragment PK datasets	2
2	Rabbit retinal geometric parameter derivations	2
3	Model Equations Conversion from pM to fmol	3
4	Model Solution	4
5	Delay model	5
6	Non-delay model individual plots	7
7	Half life and Vitreous Retina Ratio Analytic Approximation	8
8	RPE-Aqueous elimination ratio	9



1 ANTIBODY AND ANTIBODY FRAGMENT PK DATASETS

Datasets provided by Gadkar et. al. [1], detailing compartment concentration with respect to time, assuming compartment volumes, dosages and molecular weights as given in the main text. Note that for Fc was no available data in the retina but in vitreous and aqueous humor.

Time (days)	Concentration (pM)		
	Retina	Vitreous	Aqueous
0.25	1755700	6990359.8	7240.8
0.25	1368200	9393583	17088.4
0.25	8130040	7821512.8	12261.8
0.25	2617640	5723190.2	3842.2
0.25	2533400	8974832.8	53552.4
0.25	5342940	8070885.8	12993
2	3959640	5642282.6	423749.2
2	1933900	5503448.6	483301.2
2	6754200	5807142	474151.8
2	1702100	5995316.2	634976.4
2	4196860	6307667.8	440364.6
2	2517680	6610189.8	626559.4
8	683320	1085564.6	95032
8	259500	1124777.4	150671
8	184800	1744674	162597.4
8	1252700	1407034.8	174504.8
8	1045820	1515699.4	190384.4
8	703120	1118512.4	182863.8
14	377460	469199.4	51067
14	107300	498507	55237.2
14	259140	362563.8	-
14	108500	436220.6	-
14	165560	442207.2	-
14	409120	552829.2	-
21	6780	102015	-
21	44380	68507.6	-

Table S1: Fab PK dataset.

Time (days)	Concentration (pM)		
	Retina	Vitreous	Aqueous
0.25	1112756.906	2285614.6667	5658
0.25	1096043.978	2362155.3333	28447.3333
0.25	794481.51	2448978.6667	72322
0.25	1476766.09	2411743.3333	20739.3333
3	784521.176	1841156.6667	65286
3	1242283.796	1957608.6667	85434.6667
3	590948.4156	1289530	48072.6667
3	569956.3721	1704405.3333	60682
9	362641.5153	796191.3333	41487.3333
9	517955.6853	756415.3333	52070.6667
9	238365.7205	829592	58695.3333
9	421996.3525	781134	52703.3333
15	144941.973	371290	22378
15	148334.7227	351608	20994.6667
15	117563.9538	311451.3333	19520
15	150796.5086	312351.3333	18836.6667
29	16374.8635	37095.3333	2668
29	33022.748	37052.6667	2034
29	40786.4255	85031.3333	2946
29	28518.8218	78390.6667	3008

Table S3: IgG PK dataset.

Time (days)	Concentration (pM)		
	Retina	Vitreous	Aqueous
0.25	-	5907533.364	411770.6
0.25	-	4906777.11	22890.6
0.25	-	5686492.484	208261.8
0.25	-	5551086.424	187293.8
2	-	3764627.358	346021.8
2	-	3201466.3	589063.2
2	-	3705280.232	472623.4
2	-	3508841.362	687386.6
7	-	1008808.567	111683.6
7	-	1005473.5698	123491.8
7	-	874254.883	103779
7	-	898463.626	101269.4
14	-	374701.5614	32525
14	-	415425.27	39134
14	-	354738.1128	34070
14	-	303973.432	38656.4
21	-	114003.6383	10641.2
21	-	104781.7236	9533.8
21	-	46931.4242	4494.2
21	-	73358.8149	7238.6
28	-	21949.2914	2092.6
28	-	30323.5873	3234.6
28	-	24839.9355	2849
28	-	11718	1662.8

Table S2: Fc PK dataset.

Time (days)	Concentration (pM)		
	Retina	Vitreous	Aqueous
0.25	2235728.7993	2771815.3333	31452
0.25	1165834.5207	3954608	13723.3333
0.25	519135.9053	3466492	20566.6667
0.25	1295959.19	3291939.3333	6502
3	651065.5865	952232.6667	115394
3	760239.3733	2302664	106378
3	832737.8753	2131472.6667	135760.6667
3	800755.2913	2417723.3333	111032
9	365460.2451	974172.6667	47192
9	414104.6459	1105154	58171.3333
9	536251.7507	997708	54142
9	801414.1747	930590.6667	60555.3333
15	200022.7233	345246.6667	20782.6667
15	147052.6861	402230	17415.3333
15	229544.2341	466096	21278.6667
15	183210.6301	516351.3333	20178

Table S4: IgG null PK dataset.

2 RABBIT RETINAL GEOMETRIC PARAMETER DERIVATIONS

Consider the vitreous as described by a sphere, partially covered by the retina, as shown in Figure S1 below, which depicts a circular cross section through the vitreous. Using this simple geometric model we will derive estimates for  $V_{\text{ret}}$  and  $S_{\text{ret}}$ . Relevant geometric parameters are given in Table S5.

Parameter	Value	units	Description
$V_{\text{ret}}$	unknown	mL	Retinal volume
$V_{\text{vit}}$	1.52 [2]	mL	Vitreous volume
$S_{\text{ret}}$	unknown	cm <sup>2</sup>	Retinal surface area
$r$	0.713*	cm	Vitreous radius
$\epsilon$	0.01 [2]	cm	Retinal thickness
$L$	1.385 <sup>†</sup>	cm	Cross sectional arc length of retina
$\theta$	$L/r$	rad	Cross sectional sector angle

Table S5: Geometric parameters for the rabbit eye. \*The radius  $r$  is the radius of the sphere with volume  $V_{\text{vit}}$ , where the latter was taken from [2]. <sup>†</sup>This value was estimated from the scale diagrams found in [2].

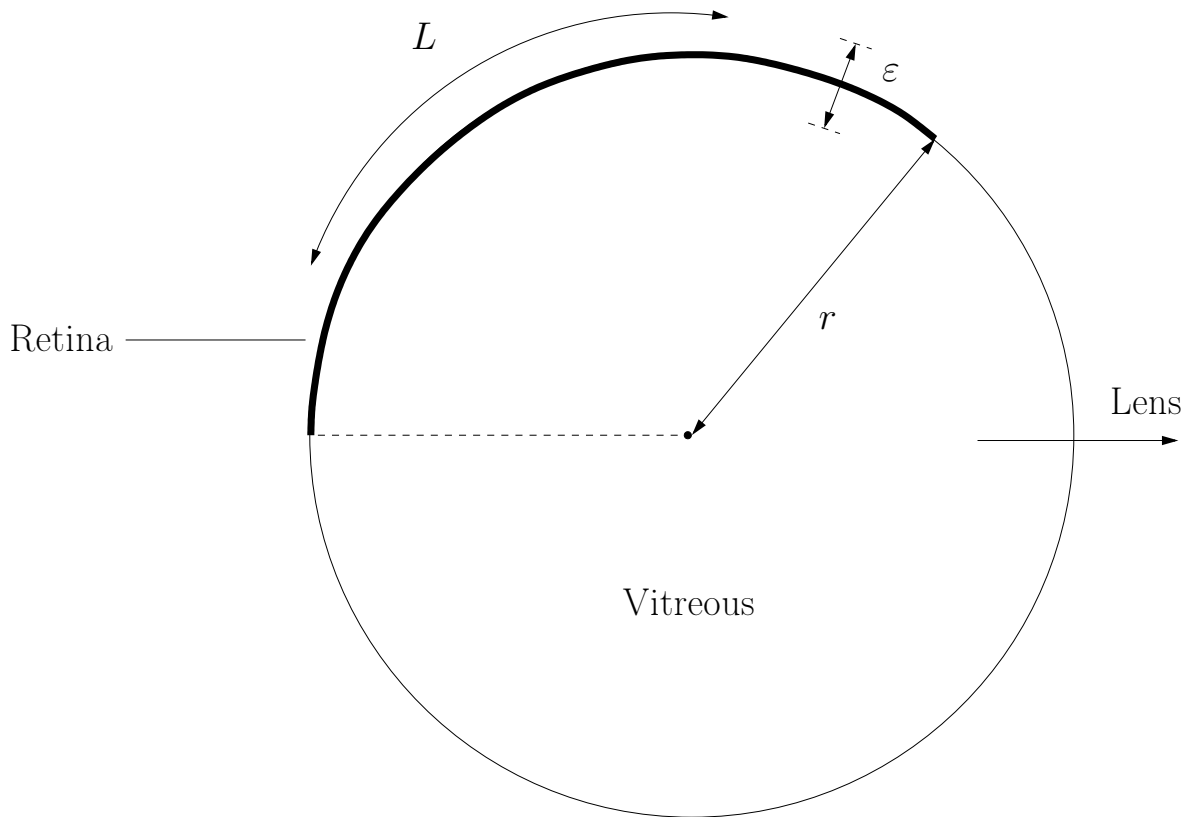


Figure S1: Geometric model used to derive parameters relating to the retina. The eye is orientated such that the lens is pointing in the positive  $x$  axis and the portion of the vitreous in contact with the retina is in bold.

Therefore, assuming azimuthal symmetry around the normal to the lens, the percentage of the vitreous in contact with the retina is given by

$$\Delta = \frac{1}{4\pi r^2} \int_0^{2\pi} \int_0^{\theta_r} r^2 \sin \theta \, d\theta d\phi \quad (\text{S.1})$$

$$= \frac{1}{2} (1 - \cos \theta_r) \quad (\text{S.2})$$

$$\approx 0.681 \quad (\text{S.3})$$

where  $\theta_r = L/r$ . Therefore we can approximate  $S_{\text{ret}}$  and  $V_{\text{ret}}$  by

$$S_{\text{ret}} = \Delta \times 4\pi r^2 \approx 4.35 \text{ cm}^2 \quad (\text{S.4})$$

$$V_{\text{ret}} = \Delta \times \frac{4}{3} \pi [(r + \epsilon)^3 - r^3] \approx 0.044 \text{ cm}^3. \quad (\text{S.5})$$

We emphasize that we assume that the surface area  $S_{\text{ret}}$  is the same on either side of the retina, i.e. for both the RPE and ILM. This approximation is reasonable due to the relative magnitudes of ocular radius ( $r$ ) and retinal thickness ( $\epsilon$ ).

### 3 MODEL EQUATIONS CONVERSION FROM PM TO FMOL

The model as described in the main text, by Equations 1-3, can be rewritten in terms of  $m_i$  as opposed to  $c_i$ , with units of fmol and pM respectively, and where the subscript  $i$  refers to the associated model compartment.  $m_i$  and  $c_i$  are related by the following expression:

$$m_i = V_i c_i \quad (\text{S.6})$$

where  $V_i$  is the volume of model compartment  $i$ , with units of mL. Equations 1-3 in the main text can now be rewritten in the following way:

$$\frac{dm_{\text{ret}}}{dt} = -\left(\frac{S_{\text{ret}}}{V_{\text{ret}}}\right) [p_{\text{ILM}} + p_{\text{RPE}}] m_{\text{ret}} + \left(\frac{S_{\text{ret}}}{V_{\text{vit}}}\right) p_{\text{ILM}} m_{\text{vit}}, \quad (\text{S.7})$$

$$\frac{dm_{\text{vit}}}{dt} = \left(\frac{S_{\text{ret}}}{V_{\text{ret}}}\right) p_{\text{ILM}} m_{\text{ret}} - \left[\left(\frac{S_{\text{ret}}}{V_{\text{vit}}}\right) p_{\text{ILM}} + k_{\text{el}}\right] m_{\text{vit}}, \quad (\text{S.8})$$

$$\frac{dm_{\text{aq}}}{dt} = k_{\text{el}} m_{\text{vit}} - \left(\frac{CL_{\text{aq}}}{V_{\text{aq}}}\right) m_{\text{aq}}, \quad (\text{S.9})$$

One can now see how each label in Figure 1 of the main text relates to a coefficient in Equations 1-3.

## 4 MODEL SOLUTION

The model as described in the main text, by Equations 1-3, is given by

$$\frac{dc_{\text{ret}}}{dt} = -\left(\frac{S_{\text{ret}}}{V_{\text{ret}}}\right) [p_{\text{ILM}} + p_{\text{RPE}}] c_{\text{ret}} + \left(\frac{S_{\text{ret}}}{V_{\text{vit}}}\right) p_{\text{ILM}} c_{\text{vit}}, \quad (\text{S.10})$$

$$\frac{dc_{\text{vit}}}{dt} = \left(\frac{S_{\text{ret}}}{V_{\text{ret}}}\right) p_{\text{ILM}} c_{\text{ret}} - \left[\left(\frac{S_{\text{ret}}}{V_{\text{vit}}}\right) p_{\text{ILM}} + k_{\text{el}}\right] c_{\text{vit}}, \quad (\text{S.11})$$

$$\frac{dc_{\text{aq}}}{dt} = \left(\frac{V_{\text{vit}}}{V_{\text{aq}}}\right) k_{\text{el}} c_{\text{vit}} - \left(\frac{CL_{\text{aq}}}{V_{\text{aq}}}\right) c_{\text{aq}}, \quad (\text{S.12})$$

where  $c_{\text{ret}}(0) = c_{\text{aq}}(0) = 0$  and  $c_{\text{vit}}(0) = c_0$  representing the initial concentration corresponding to the intravitreal injection. All parameter definitions can be found in Table 2 in the main text. As this is a linear ODE system with constant coefficients, it is readily solved to give:

$$c_{\text{ret}}(t) = \frac{c_0 p_{\text{ILM}}}{\lambda_2 - \lambda_1} \left(\frac{S_{\text{ret}}}{V_{\text{vit}}}\right) K_2 K_1 \left[e^{-\lambda_1 t} - e^{-\lambda_2 t}\right], \quad (\text{S.13})$$

$$c_{\text{vit}}(t) = \frac{c_0 p_{\text{ILM}}}{\lambda_2 - \lambda_1} \left(\frac{S_{\text{ret}}}{V_{\text{vit}}}\right) \left[K_1 e^{-\lambda_2 t} + K_2 e^{-\lambda_1 t}\right], \quad (\text{S.14})$$

$$c_{\text{aq}}(t) = \frac{c_0 p_{\text{ILM}} k_{\text{el}}}{\lambda_2 - \lambda_1} \left(\frac{S_{\text{ret}}}{V_{\text{aq}}}\right) \left[ \frac{K_1}{\frac{CL_{\text{aq}}}{V_{\text{aq}}} - \lambda_2} \left(e^{-\lambda_2 t} - e^{-\left(\frac{CL_{\text{aq}}}{V_{\text{aq}}}\right)t}\right) + \frac{K_2}{\frac{CL_{\text{aq}}}{V_{\text{aq}}} - \lambda_1} \left(e^{-\lambda_1 t} - e^{-\left(\frac{CL_{\text{aq}}}{V_{\text{aq}}}\right)t}\right) \right], \quad (\text{S.15})$$

where

$$K_1 = 1 + \left(\frac{V_{\text{vit}}}{S_{\text{ret}}}\right) \frac{k_{\text{el}} - \lambda_1}{p_{\text{ILM}}}, \quad K_2 = -1 + \left(\frac{V_{\text{vit}}}{S_{\text{ret}}}\right) \frac{\lambda_2 - k_{\text{el}}}{p_{\text{ILM}}}, \quad (\text{S.16})$$

and  $\lambda_1, \lambda_2$  are defined as

$$\lambda_1 = -\frac{1}{2} \left( \text{Tr}(M) + \sqrt{\text{Tr}(M)^2 - 4 \det M} \right), \quad (\text{S.17})$$

$$\lambda_2 = -\frac{1}{2} \left( \text{Tr}(M) - \sqrt{\text{Tr}(M)^2 - 4 \det M} \right), \quad (\text{S.18})$$

where  $K_1, K_2, \lambda_1, \lambda_2 > 0$ , with  $M$  defined as

$$M = \begin{pmatrix} -\frac{S_{\text{ret}}}{V_{\text{ret}}} (p_{\text{ILM}} + p_{\text{RPE}}) & \frac{S_{\text{ret}}}{V_{\text{ret}}} p_{\text{ILM}} \\ \frac{S_{\text{ret}}}{V_{\text{vit}}} p_{\text{ILM}} & -\left(\frac{S_{\text{ret}}}{V_{\text{vit}}} p_{\text{ILM}} + k_{\text{el}}\right) \end{pmatrix}. \quad (\text{S.19})$$

From Table 2 in the main text, we have that  $\lambda_1 / \lambda_2 \simeq 0.05 \ll 1$ . In this case we can approximate the long time ( $t \sim O(1/\lambda_1)$ ) behavior of the system in the retina and vitreous by the following equations

$$c_{\text{ret}}(t) \simeq \frac{c_0 p_{\text{ILM}}}{\lambda_2 - \lambda_1} \left(\frac{S_{\text{ret}}}{V_{\text{vit}}}\right) K_2 K_1 e^{-\lambda_1 t}, \quad (\text{S.20})$$

$$c_{\text{vit}}(t) \simeq \frac{c_0 p_{\text{ILM}}}{\lambda_2 - \lambda_1} \left(\frac{S_{\text{ret}}}{V_{\text{vit}}}\right) K_2 e^{-\lambda_1 t}, \quad (\text{S.21})$$

$$c_{\text{aq}}(t) \simeq \frac{c_0 p_{\text{ILM}} k_{\text{el}}}{\lambda_2 - \lambda_1} \left(\frac{S_{\text{ret}}}{V_{\text{aq}}}\right) \left( \frac{K_2}{\frac{CL_{\text{aq}}}{V_{\text{aq}}} - \lambda_1} \right) e^{-\lambda_1 t}. \quad (\text{S.22})$$

Therefore the long-time vitreous retina concentration ratio is given by

$$R_{VR} \simeq \frac{1}{K_1}. \quad (\text{S.23})$$

Note, for readers unfamiliar with the terms  $\det$  and  $\text{Tr}$ , we have defined then below, for a 2x2 matrix  $M$ , defined as

$$M = \begin{pmatrix} a & b \\ c & d \end{pmatrix} \quad (\text{S.24})$$

then  $\det M$  and  $\text{Tr}(M)$  are defined as:

$$\det M = ad - bc \quad (\text{S.25})$$

$$\text{Tr}(M) = a + d \quad (\text{S.26})$$

## 5 DELAY MODEL

The delay model is given by the following linear system

$$\frac{dc_{\text{ret}}}{dt} = \frac{S_{\text{ret}}}{V_{\text{ret}}} [-(p_{\text{ILM}} + p_{\text{RPE}})c_{\text{ret}} + p_{\text{ILM}}c_{\text{vit}}], \quad (\text{S.27})$$

$$\frac{dc_{\text{vit}}}{dt} = \left(\frac{S_{\text{ret}}}{V_{\text{vit}}}\right)p_{\text{ILM}}c_{\text{ret}} - \left(\left(\frac{S_{\text{ret}}}{V_{\text{vit}}}\right)p_{\text{ILM}} + k_{\text{el}}\right)c_{\text{vit}}, \quad (\text{S.28})$$

$$\frac{dc_{\mu}}{dt} = \left(\frac{V_{\text{vit}}}{V_{\text{aq}}}\right)k_{\text{el}}c_{\text{vit}} - \mu c_{\mu}, \quad (\text{S.29})$$

$$\frac{dc_{\text{aq}}}{dt} = \mu c_{\mu} - \left(\frac{CL_{\text{aq}}}{V_{\text{aq}}}\right)c_{\text{aq}}, \quad (\text{S.30})$$

where  $c_{\text{ret}}(0) = c_{\mu}(0) = c_{\text{aq}}(0) = 0$  and  $c_{\text{vit}}(0) = c_0$  representing the initial concentration corresponding to the intravitreal injection, and where  $\mu$  (with units of 1/day) is the rate of transfer from the virtual delay compartment into the aqueous, as shown in Figure S2.

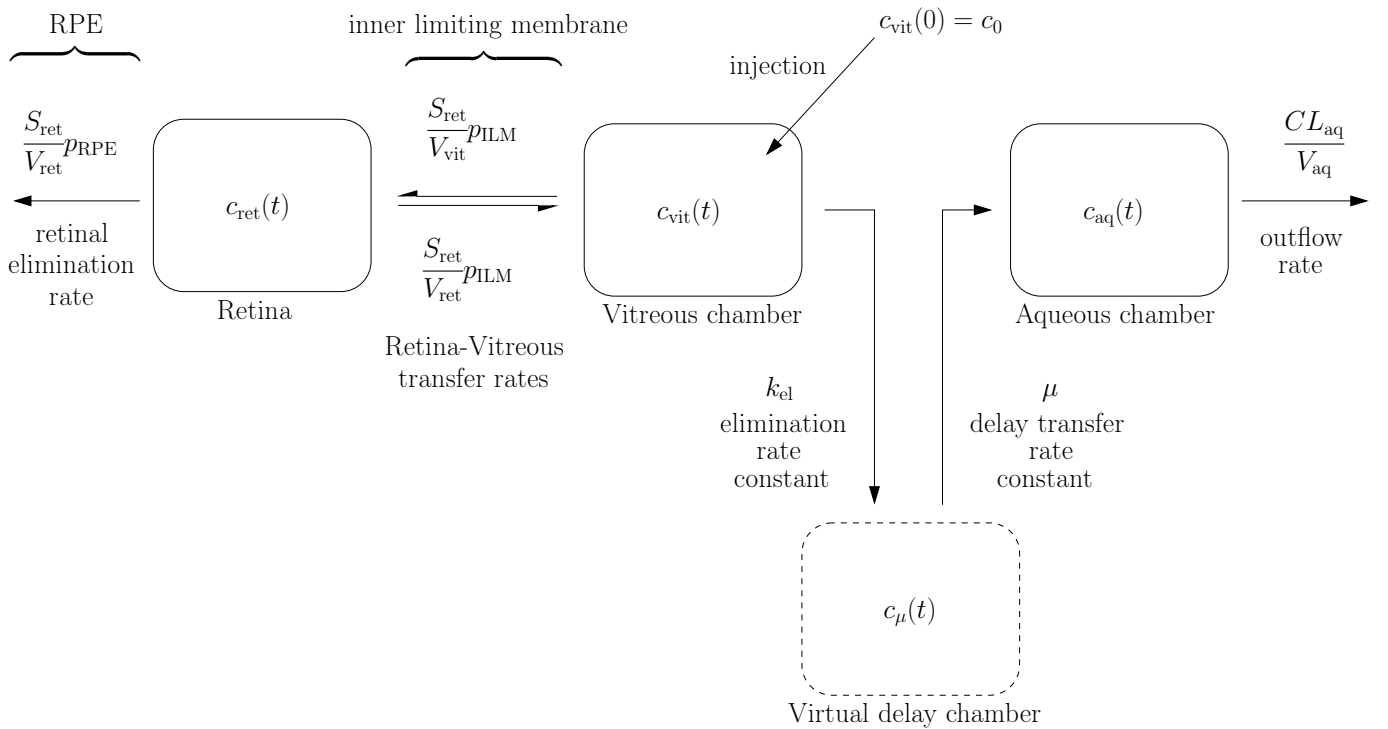


Figure S2: 3-compartment PK model for a general antibody, with concentration  $c(t)$ , injected into the vitreous chamber and which may transit from the vitreous into the aqueous or retina. Subscripts on  $c(t)$  indicate the notation for each compartments respective concentration. Note the virtual delay compartment, separating the vitreous and the aqueous; for large values of  $\mu$  we can consider the model as not to include this virtual compartment.

Parameter	Non-delay model				Delay model				Units
	Fab	Fc	IgG	IgG null	Fab	Fc	IgG	IgG null	
$p_{\text{RPE}} (\times 10^{-7})$	2.60 (1.36, 4.04)	n/a	1.84 (1.08, 2.36)	1.91 (1.07, 2.50)	2.71 (1.38, 4.39)	n/a	1.86 (1.10, 2.45)	2.34 (1.34, 3.20)	cm/sec
$p_{\text{ILM}} (\times 10^{-7})$	1.88 (1.13, 2.81)	n/a	1.70 (0.912, 2.32)	1.65 (0.758, 2.52)	2.12 (1.26, 3.34)	n/a	1.87 (1.06, 2.64)	2.05 (1.02, 3.14)	cm/sec
$\frac{p_{\text{RPE}}}{p_{\text{ILM}}}$	1.38 (0.71, 2.21)	n/a	1.08 (0.61, 1.57)	1.16 (0.65, 1.64)	1.27 (0.66, 2.02)	n/a	0.99 (0.54, 1.45)	1.14 (0.69, 1.59)	none
$k_{\text{el}}$	0.197 (0.179, 0.219)	0.169 (0.161, 0.178)	0.107 (0.0985, 0.119)	0.118 (0.109, 0.131)	0.200 (0.18, 0.225)	0.173 (0.165, 0.184)	0.109 (0.1, 0.122)	0.117 (0.106, 0.131)	1/day
$\mu$	n/a	n/a	n/a	n/a	0.765 (0.468, 1.42)	1.61 (0.589, 2.5)	1.12 (0.42, 2.5)	0.674 (0.441, 1.24)	1/day
$\lambda_1$	0.223	0.196	0.128	0.139	0.228	0.20	0.131	0.143	1/day
$\lambda_2$	3.84	3.96	3.04	3.06	4.14	4.00	3.21	3.76	1/day
$t_{1/2}$	3.11	3.54	5.42	4.98	3.04	3.47	5.30	4.86	days

Table S6: Optimized parameter summary across delay and non-delay models, including 95% confidence intervals obtained via Monte Carlo simulations using error bootstrapping. Due to the lack of retinal data for molecule Fc, estimate for pRPE, pILM and hence their ratio were not able to be obtained.

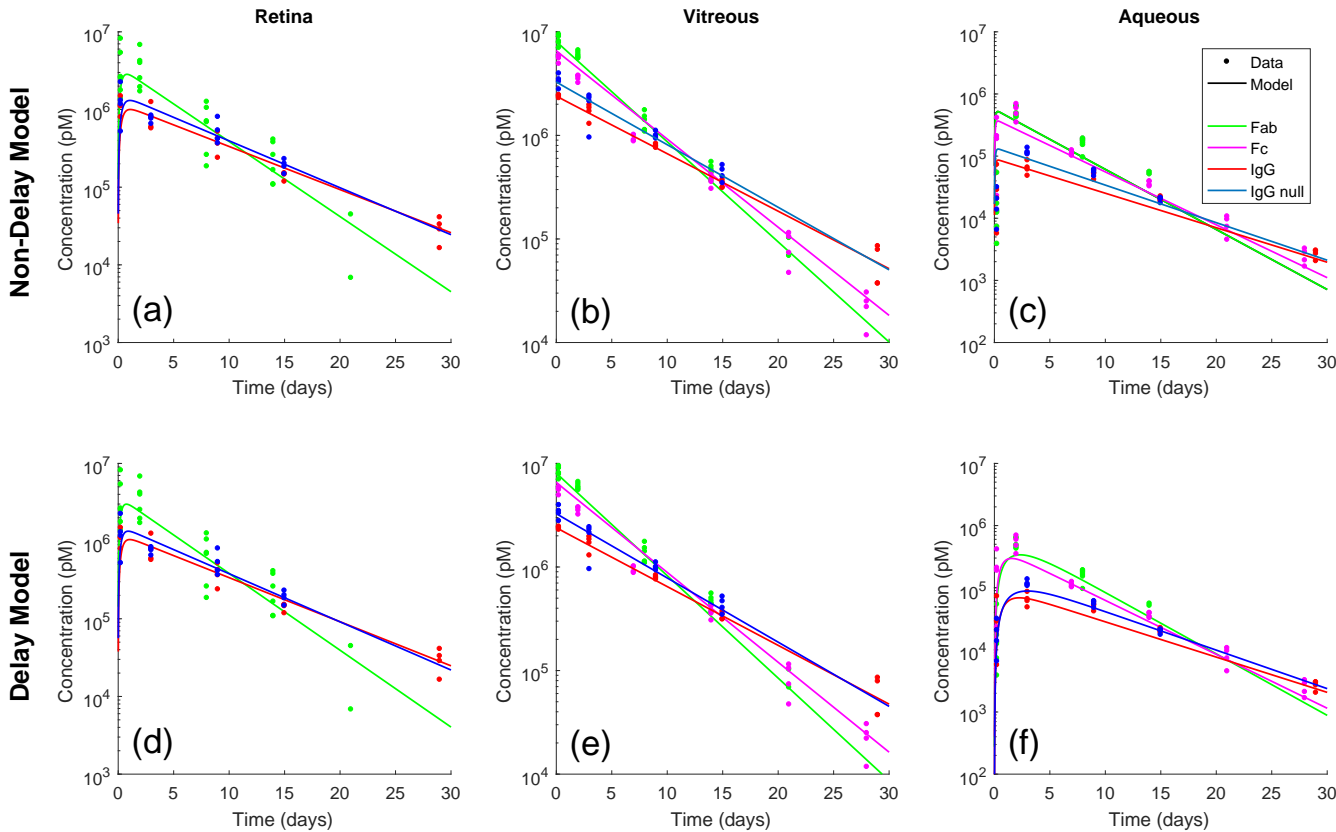


Figure S3: Compilation of optimized fits to the dataset [1]. Colored markers indicate distinct molecule data sets, whereas colored lines show the optimized fit. (a-c) were fit using the non-delay model and (d-f) using the delay model. Note that there was no available data for Fc in the retina, this dataset was fit purely using vitreous and aqueous data.

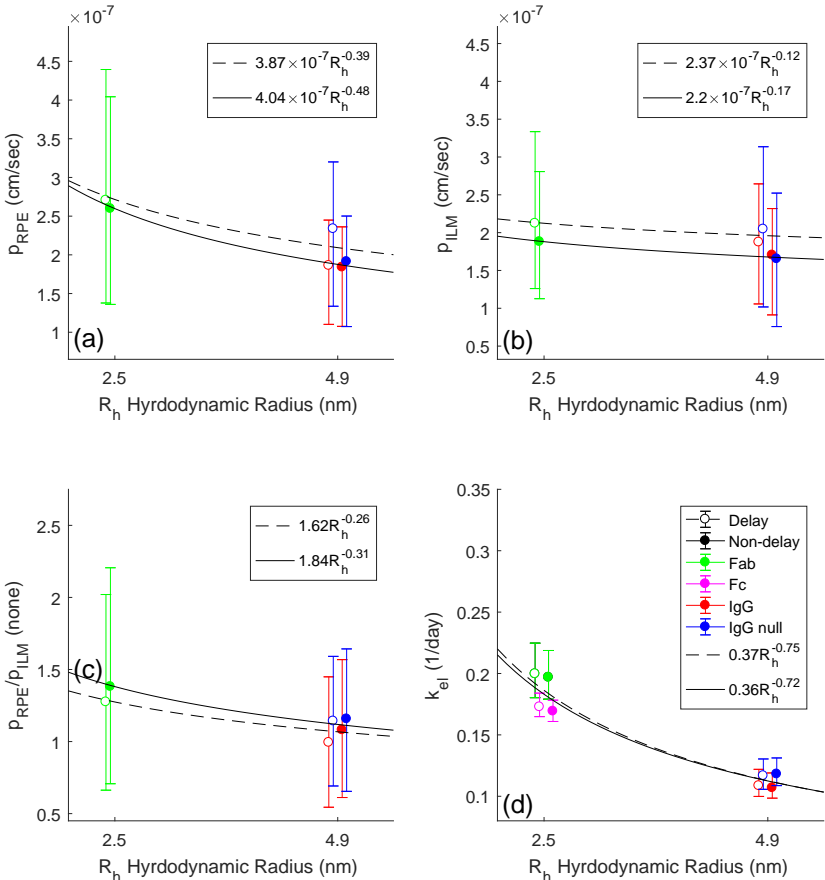


Figure S4: Optimized parameters across delay and non-delay models, unfilled and solid markers respectively, plotted with respect to hydrodynamic radius ( $R_h$ ).

As for the non-delay model, Equations S.31-S.35 define a linear ODE system with constant coefficients, with solution for the concentrations of the retina, vitreous and aqueous:

$$c_{\text{ret}}(t) = \frac{c_0 p_{\text{ILM}}}{\lambda_2 - \lambda_1} \left( \frac{S_{\text{ret}}}{V_{\text{vit}}} \right) K_2 K_1 \left[ e^{-\lambda_1 t} - e^{-\lambda_2 t} \right], \quad (\text{S.31})$$

$$c_{\text{vit}}(t) = \frac{c_0 p_{\text{ILM}}}{\lambda_2 - \lambda_1} \left( \frac{S_{\text{ret}}}{V_{\text{vit}}} \right) \left[ K_1 e^{-\lambda_2 t} + K_2 e^{-\lambda_1 t} \right], \quad (\text{S.32})$$

$$c_{\text{aq}}(t) = \frac{c_0 p_{\text{ILM}} k_{\text{el}}}{\lambda_2 - \lambda_1} \left( \frac{S_{\text{ret}}}{V_{\text{aq}}} \right) \left[ \frac{1}{\frac{CL_{\text{aq}}}{V_{\text{aq}}} - \lambda_2} \frac{K_1}{1 - \lambda_2/\mu} \left( e^{-\lambda_2 t} - e^{-\left(\frac{CL_{\text{aq}}}{V_{\text{aq}}}\right)t} \right) \right. \quad (\text{S.33})$$

$$+ \left( \frac{1}{\frac{CL_{\text{aq}}}{V_{\text{aq}}} - \lambda_1} \right) \left( \frac{K_2}{1 - \lambda_1/\mu} \right) \left( e^{-\lambda_1 t} - e^{-\left(\frac{CL_{\text{aq}}}{V_{\text{aq}}}\right)t} \right) \quad (\text{S.34})$$

$$\left. - \frac{1}{\frac{CL_{\text{aq}}}{V_{\text{aq}}} - \mu} \left[ \frac{K_1}{1 - \lambda_2/\mu} + \frac{K_2}{1 - \lambda_1/\mu} \right] \left( e^{-\mu t} - e^{-\left(\frac{CL_{\text{aq}}}{V_{\text{aq}}}\right)t} \right) \right], \quad (\text{S.35})$$

where

$$K_1 = 1 + \left( \frac{V_{\text{vit}}}{S_{\text{ret}}} \right) \frac{k_{\text{el}} - \lambda_1}{p_{\text{ILM}}}, \quad K_2 = -1 + \left( \frac{V_{\text{vit}}}{S_{\text{ret}}} \right) \frac{\lambda_2 - k_{\text{el}}}{p_{\text{ILM}}}, \quad (\text{S.36})$$

and  $\lambda_1, \lambda_2$  are defined as

$$\lambda_1 = -\frac{1}{2} \left( \text{Tr}(M) + \sqrt{\text{Tr}(M)^2 - 4 \det M} \right), \quad (\text{S.37})$$

$$\lambda_2 = -\frac{1}{2} \left( \text{Tr}(M) - \sqrt{\text{Tr}(M)^2 - 4 \det M} \right), \quad (\text{S.38})$$

$$M = \begin{pmatrix} -\frac{S_{\text{ret}}}{V_{\text{ret}}} (p_{\text{ILM}} + p_{\text{RPE}}) & \frac{S_{\text{ret}}}{V_{\text{ret}}} p_{\text{ILM}} \\ \frac{S_{\text{ret}}}{V_{\text{vit}}} p_{\text{ILM}} & -\left( \frac{S_{\text{ret}}}{V_{\text{vit}}} p_{\text{ILM}} + k_{\text{el}} \right) \end{pmatrix}. \quad (\text{S.39})$$

Figure S3 shows optimized fits (of the delay and non-delay model) for the retina, vitreous and aqueous data sets from Gadkar et. al. 2015, obtained using the fitting protocol described in the methods section. A summary of the optimized parameters and confidence intervals for both models can be found in Table 5, as well as in Figure S4.

The retinal and vitreal compartments are almost identical for the non-delay (a-c) and delay (d-f) models, the major difference between the two models appears in the aqueous compartment. The addition of the virtual delay compartment introduces a post transient peak (on a timescale of the order of  $1/\lambda$ ) in the aqueous compartment, allowing the curve to pass through the initial aqueous data points as  $t = 0.25$  days.

In contrast the non-delay model was found to not be able to be fit accurately with the inclusion of these initial aqueous data points, motivating the need for the delay term. However by excluding the data corresponding to  $t = 0.25$  days during the fitting protocol the non-delay model could not only be fit successfully, but returned very similar parameter values as the delay model, without the need for the introduction of the additional delay parameter  $\mu$ , as can be seen in Table S4. As can be seen from Figure S4 the optimized parameters for the delay and non-delay models also indicate similar parameter dependencies on hydrodynamic radius.

## 6 NON-DELAY MODEL INDIVIDUAL PLOTS

See below in Figure S5 the optimized model fits to [1], from Figure 2 in the main text, plotted individually by molecule.

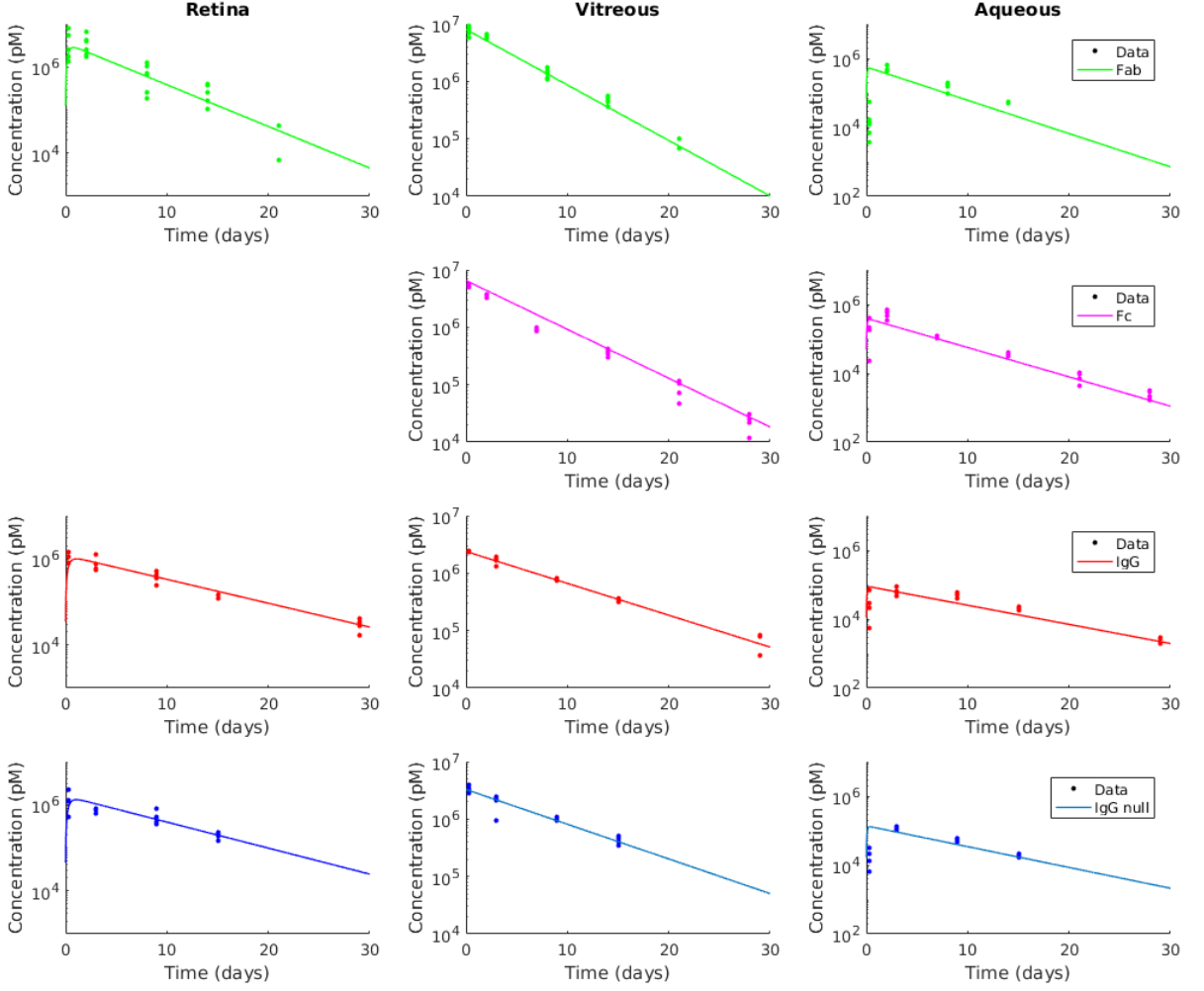


Figure S5: Individual molecule plots, as seen in Figure 2 from the main text.

## 7 HALF LIFE AND VITREOUS RETINA RATIO ANALYTIC APPROXIMATION

As we find  $\lambda_1 \ll \lambda_2$ , we can write the following relation

$$t_{1/2} = \frac{\log 2}{\lambda_1}, \quad (\text{S.40})$$

where  $t_{1/2}$  is the drug half-life. This motivates a deeper understanding of the analytic expression  $\lambda_1$ , presented below. First let us examine the following expression,

$$\sqrt{\text{Tr}(M)^2 - 4 \det M} = \sqrt{\left[ \frac{S_{\text{ret}}}{V_{\text{ret}}} \left( \left( 1 - \frac{V_{\text{ret}}}{V_{\text{vit}}} \right) p_{\text{ILM}} + p_{\text{RPE}} \right) - k_{\text{el}} \right]^2 + 4 \frac{(S_{\text{ret}} p_{\text{ILM}})^2}{V_{\text{ret}} V_{\text{vit}}}} \quad (\text{S.41})$$

$$= \left[ \frac{S_{\text{ret}}}{V_{\text{ret}}} \left( \left( 1 - \frac{V_{\text{ret}}}{V_{\text{vit}}} \right) p_{\text{ILM}} + p_{\text{RPE}} \right) - k_{\text{el}} \right] \sqrt{1 + \underbrace{\left( \frac{V_{\text{ret}}}{V_{\text{vit}}} \right)}_{\ll 1} \underbrace{\left[ \frac{2}{1 + \frac{p_{\text{RPE}}}{p_{\text{ILM}}} - \frac{V_{\text{ret}}}{V_{\text{vit}}} \left( 1 + \frac{V_{\text{vit}} k_{\text{el}}}{S_{\text{ret}} p_{\text{ILM}}} \right)} \right]}_{\sim O(1)}}^2}. \quad (\text{S.42})$$

In Equation S.42 note that, given Table 2 in the main text,  $V_{\text{ret}} \ll V_{\text{vit}}$ , allowing us to make the following approximation

$$\sqrt{\text{Tr}(M)^2 - 4 \det M} \simeq \left[ \frac{S_{\text{ret}}}{V_{\text{ret}}} \left( \left( 1 - \frac{V_{\text{ret}}}{V_{\text{vit}}} \right) p_{\text{ILM}} + p_{\text{RPE}} \right) - k_{\text{el}} \right] \left( 1 + \left( \frac{V_{\text{ret}}}{V_{\text{vit}}} \right) \frac{2}{\left[ 1 + \frac{p_{\text{RPE}}}{p_{\text{ILM}}} - \frac{V_{\text{ret}}}{V_{\text{vit}}} \left( 1 + \frac{V_{\text{vit}} k_{\text{el}}}{S_{\text{ret}} p_{\text{ILM}}} \right) \right]^2} \right). \quad (\text{S.43})$$

Therefore  $\lambda_1$  can be approximated by

$$\lambda_1 \simeq k_{\text{el}} + \left( \frac{S_{\text{ret}} p_{\text{ILM}}}{V_{\text{vit}}} \right) - \frac{1}{1 + \frac{p_{\text{RPE}}}{p_{\text{ILM}}} - \frac{V_{\text{ret}}}{V_{\text{vit}}} \left( 1 + \frac{V_{\text{vit}} k_{\text{el}}}{S_{\text{ret}} p_{\text{ILM}}} \right)} \left( \frac{S_{\text{ret}} p_{\text{ILM}}}{V_{\text{vit}}} \right). \quad (\text{S.44})$$

Therefore using this approximation we may now express Equation S.23 as the following

$$R_{VR} \simeq 1 + \frac{p_{RPE}}{p_{ILM}} - \frac{V_{ret}}{V_{vit}} \left( 1 + \frac{V_{vit} k_{el}}{S_{ret} p_{ILM}} \right) \quad (S.45)$$

via the definition of  $K_1$  given in Equation S.16a.

Note, if

$$1 + \frac{p_{RPE}}{p_{ILM}} \gg \frac{V_{ret}}{V_{vit}} \left( 1 + \frac{V_{vit} k_{el}}{S_{ret} p_{ILM}} \right), \quad (S.46)$$

a plausible assumption due to the relative volumes of the vitreous and retina, then we can approximate Equation S.45 by the following expression

$$R_{VR} \simeq 1 + \frac{p_{RPE}}{p_{ILM}}, \quad (S.47)$$

and similarly write

$$\lambda_1 \simeq k_{el} + \left( \frac{S_{ret} p_{ILM}}{V_{vit}} \right) - \underbrace{\frac{1}{1 + \frac{p_{RPE}}{p_{ILM}}}}_{\simeq R_{VR}} \left( \frac{S_{ret} p_{ILM}}{V_{vit}} \right) \quad (S.48)$$

Molecule	Fab	IgG	IgG null
Exact value of $R_{VR}$	2.26	2.01	2.08
Accuracy of Equation S.45	99.48%	99.35%	99.39%
Accuracy of Equation S.47	94.40%	95.95%	95.67%
Exact value of $\lambda_1$	0.2224	0.1278	0.1387
Accuracy of Equation S.44	99.95%	99.90%	99.92%
Accuracy of Equation S.48	99.51%	99.38%	99.42%

Table S7: Accuracy summary of the approximations made in Section 7. All accuracies are given relative to their respective exact value, generated from the exact analytic solution.

## 8 RPE-AQUEOUS ELIMINATION RATIO

The approximate number of molecules (given in pmols) which exit via the RPE and via the aqueous are given, respectively, by

$$E_{RPE} = S_{ret} p_{RPE} \int_0^\infty c_{ret}(s) ds \simeq S_{ret} p_{RPE} K_1 \left( \frac{S_{ret}}{V_{vit}} \frac{c_0 p_{ILM} K_2}{\lambda_1 (\lambda_2 - \lambda_1)} \right), \quad (S.49)$$

$$E_{aq} = k_{el} V_{vit} \int_0^\infty c_{vit}(s) ds \simeq k_{el} V_{vit} \left( \frac{S_{ret}}{V_{vit}} \frac{c_0 p_{ILM} K_2}{\lambda_1 (\lambda_2 - \lambda_1)} \right), \quad (S.50)$$

where the integral coefficients are the elimination rates from the vitreous to the aqueous and retina to the choroid, respectively. Therefore, noting that  $K_1 = 1/R_{VR}$ , their ratio is given approximately by

$$\frac{E_{aq}}{E_{RPE}} \simeq \frac{k_{el} V_{vit}}{S_{ret} p_{RPE}} \left( 1 + \frac{p_{RPE}}{p_{ILM}} \right). \quad (S.51)$$

## REFERENCES

- [1] Kapil Gadkar, Cinthia V. Pastuskovas, Jennifer E. Le Couter, J. Michael Elliott, Jianhuan Zhang, Chingwei V. Lee, Sarah Sanowar, Germaine Fuh, Hok Seon Kim, T. Noelle Lombana, Christoph Spiess, Makia Nakamura, Phil Hass, Whitney Shatz, Y. Gloria Meng, and Justin M. Scheer. Design and Pharmacokinetic Characterization of Novel Antibody Formats for Ocular Therapeutics. *Investigative Ophthalmology & Visual Science*, 56(9):5390–5400, 2015.
- [2] Paul J. Missel. Simulating intravitreal injections in anatomically accurate models for rabbit, monkey, and human eyes. *Pharmaceutical Research*, 29(12):3251–3272, 2012.